arXiv:2505.09088v1 [math.OC] 14 May 2025

Derivative-free optimization is competitive for aerodynamic design optimization in moderate dimensions

Punya Plaban*[1], Peter Bachman†[1], and Ashwin Renganathan‡[1,2]

[1]The Pennsylvania State University, University Park, PA, 16802
[2]Penn State Institute of Computational and Data Sciences, University Park, PA, 16802

Abstract

Aerodynamic design optimization is an important problem in aircraft design that depends on the interplay between a numerical optimizer and a high-fidelity flow physics solver. Derivative-based, first and (quasi) second order, optimization techniques are the de facto choice, particularly given the availability of the adjoint method and its ability to efficiently compute gradients at the cost of just one solution of the forward problem. However, implementation of the adjoint method requires careful mathematical treatment, and its sensitivity to changes in mesh quality limits widespread applicability. Derivative-free approaches are often overlooked for large scale optimization, citing their lack of scalability in higher dimensions and/or the lack of practical interest in globally optimal solutions that they often target. However, breaking free from an adjoint solver can be paradigm-shifting in broadening the applicability of aerodynamic design optimization. We provide a systematic benchmarking of a select sample of widely used derivative-based and derivative-free optimization algorithms on the design optimization of three canonical aerodynamic bodies, namely, the NACA0012 and RAE2822 airfoils, and the ONERAM6 wing. Our results demonstrate that derivative-free methods are competitive with derivative-based methods, while outperforming them consistently in the high-dimensional setting. These findings highlight the practical competitiveness of modern derivative-free strategies, offering a scalable and robust alternative for aerodynamic design optimization when adjoint-based gradients are unavailable or unreliable.

1 Introduction

The environmental impact of aircraft, via reduced fuel burn, is achieved primarily by optimizing the aircraft wing and control surface shapes for better aerodynamic efficiency (e.g.,

*Graduate assistant, Aerospace Engineering, 556 White Course drive.
†Undergraduate research assistant, Aerospace Engineering, 556 White Course drive.
‡Assistant professor, Aerospace Engineering, 556 White Course drive. Corresponding author.

higher lift-drag ratios). Aerodynamic shape optimization (ASO), which refers to optimizing parametrized shapes of aerodynamic bodies for aerodynamic performance, under various constraints, is a popular and active research area [31]. Solving this optimization problem with a high-fidelity computational fluid dynamics (CFD) model of the aircraft makes it computationally demanding; this is further exacerbated by the dimensionality of the parametrization. Derivative-based optimization, with sensitivities computed via the adjoint method [19], makes high-fidelity gradient computation feasible at only an additional cost of one primal (forward) solution. Therefore, derivative-based approach to ASO is considered the most scalable approach and hence is the gold standard. However, this consideration is underpinned by the assumption that a robust adjoint formulation and an associated adjoint solver are available. First, implementation of the adjoint method for high-fidelity CFD solvers requires careful mathematical treatment and an involved numerical implementation. Second, convergence of adjoint solvers can be very sensitive to mesh quality and changes in boundary conditions [31, 32]. Third, the adjoint solve still costs as much as the forward solve—practically speaking, derivative-based algorithms require multiple gradient evaluations per step, to compute appropriate step lengths or for Hessian approximation, which can get prohibitively expensive. Renganathan et al. [48] showed that gradient-free approaches can be $10\times$ computationally cheaper than adjoint-based approaches for ASO. Finally, in the presence of non-computable constraints, such as due to numerical divergence, derivative-based methods often lack robustness [21]. Given these challenges, despite the benefits of adjoint-based approaches, we are interested in exploring derivative-free approaches to ASO that could potentially widen its applicability. One case in point is ASO with large eddy simulations (LES) which better captures high angle-of-attack flows (e.g., takeoff and landing) where adjoints are inherently stochastic—approximations may be required such as using time-averaged states to compute the adjoints. Another example is chemically reacting flows in the hypersonic regime where the time scales for flow, chemistry, and heat transfer can be highly disparate, making adjoint computation challenging. While the need for derivative-free ASO is compelling, the question that remains is: *are derivative-free approaches scalable for ASO?* We intend to address this question systematically in this work. Generally speaking, derivative-free methods, such as Nelder-Mead [36], COBYLA [40], and DIRECT [22], are at a disadvantage due to the additional work they have to do to identify descent directions in the absence of derivative information. However, surrogate-based "global optimization" approaches, such as Bayesian optimization [44, 10, 11], exploit knowledge gained on the design space through a data-driven global surrogate model. Our focus here is primarily on pitting a surrogate-based approach, such as `BO`, against the classic adjoint-based method for ASO; however, we also include classic derivative-free methods, Nelder-Mead and COBYLA, in this study.

Surrogate-based approaches to aerodynamic optimization are not new. Arguably, Gaussian process (GP) regression [44] is the most popular choice of surrogates, which, along with a Bayesian decision-theoretic framework, leads to what is called "Bayesian optimization"–a popular derivative-free optimization method. Liu et al. [29] showed that multiobjective Bayesian optimization (MOBO) can be applied effectively to airfoil shape optimization, achieving high-quality Pareto fronts with minimal CFD evaluations. Gradient-enhanced Bayesian optimization has been shown to be competitive with quasi-Newton optimizers such as SNOPT [31]. However, it is not clear if, in the presence of derivative information, one is better off sticking to classic derivative-based line search or trust-region methods. Reist et al. [45]

highlights the potential benefit of combining global and local search strategies for better results. BO has also been successfully applied to conceptual aircraft design problems with hidden constraints, such as simulation failures, by leveraging machine-learning classifiers to improve optimization reliability [21], in reliability analysis [46]. Other applications include active flow control [21], multifidelity optimization [57, 7, 49], and chance-constrained optimization [24].

Recent advances have integrated deep learning techniques into surrogate-based aerodynamic optimization to address challenges related to high-dimensional scaling. Li et al. [27] proposed a framework combining deep convolutional generative adversarial networks (DCGAN) to generate realistic airfoil and wing shapes with a convolutional neural network (CNN)-based discriminator to filter out geometrically invalid samples – this led to an efficient low-dimensional parametrization. Building on the potential of generative models, Chen et al. [5] introduced a Bézier-GAN framework that learns a low-dimensional latent space of airfoil geometries, which is then wrapped into a Bayesian optimizer. In a related effort, Sheikh et al. [52] a Design-by-Morphing (DbM) strategy with a mixed-variable multi-objective Bayesian optimization (MixMOBO) algorithm. The DbM approach enables exploration across a rich design space by morphing between baseline geometries, while MixMOBO efficiently navigates this space using a portfolio of acquisition functions and batch evaluations. Another work uses partial least squares with Kriging surrogates to tackle high-dimensional scaling [4]. Queipo et al. [41] and Li et al. [28] provide comprehensive reviews of surrogate-based approaches.

Overall, we observe several gaps in the existing work. First, to our knowledge, a systematic comparison between classic derivative-based methods and derivative-free methods doesn't exist. Specifically, comparisons in terms of convergence rate, achieving optimality, and sample efficiency are lacking. Second, existing work generally applies surrogate-based methods to specific application problems. However, evaluating them on a suite of problems of varying characteristics and a consistent comparison against derivative-based methods is likely to offer better insights into the viability of derivative-free methods for aerodynamic optimization. In this work, we leverage canonical aerodynamic shape optimization problems which standardizes the benchmarking exercise. Our objective is to address the aforementioned gaps; however, our study has limited scope that we clarify below:

Remark 1. Our choice of derivative-based and derivative-free algorithms for benchmarking is by no means exhaustive. However, we select algorithms that are widely found in well-established open-source optimization libraries, and we ensure there is sufficient diversity in their respective methodologies.

Remark 2. Our study is not an evaluation of global versus local optimization approaches to ASO. Rather, we are interested in the practical utility of derivative-free approaches to ASO. In this regard, we entertain both local and global derivative-free approaches in this study.

Remark 3. As a first step, we restrict ourselves to moderate dimensions (< 50); higher dimensional investigation is reserved for future work.

The rest of the article is organized as follows. In Section 2, we provide details of the optimization problem, aerodynamic model, and the experiment design. In Section 3, we present the results and the associated discussion. We conclude in Section 4 with an outlook for future work.

2 Optimization problem

We are interested in solving aerodynamic design optimization problems that fall under the following generic class of nonlinear programming

$$\begin{aligned} \min_{\mathbf{x}\in\mathcal{X}\subset\mathbb{R}^n} & f(\mathbf{x}) \\ \text{s.t. } & c_i(\mathbf{x}) = 0,\ \forall\ i \in \mathcal{E} \\ & c_i(\mathbf{x}) \geq 0,\ \forall i \in \mathcal{I}, \end{aligned} \tag{1}$$

where $f : \mathbb{R}^n \to \mathbb{R}$ is the objective function, $c_i : \mathbb{R}^n \to \mathbb{R}$ are constraint functions, and $\mathcal{E}$ and $\mathcal{I}$ are the sets of indices representing equality and inequality constraints, respectively, $\mathbf{x} \in \mathcal{X}$ are the design variables and $\mathcal{X} \subset \mathbb{R}^n$ is a compact domain. In aerodynamic design, the objective function is the drag coefficient; the constraints involve the aerodynamic lift and moment coefficients in addition to the thickness of the geometry. The design variables $\mathbf{x}$ are the free-form deformation (FFD) [18, 50] control point displacements as described in Section 2.1. The aerodynamic coefficients that are part of the objectives and constraints of (1) are computed via computational fluid dynamics, which is explained in the following section.

Let $\Omega \subset \mathcal{X}$ denote the feasible set. Then, derivative-based methods typically generate a sequence of iterates according to

$$\mathbf{x}_{k+1} = \mathbf{x}_k + \alpha_k \mathbf{p}_k,\ k = 0, 1, 2, \ldots \tag{2}$$

where $\mathbf{x}_k$ denotes the kth iterate, α_k and $\mathbf{p}_k$ are the step length and search direction at the kth iterate, respectively, and $\mathbf{x}_0$ is typically a user-provided "guess". The search direction $\mathbf{p}_k$ is some function of the gradient of the objective and constraints, and if α_k is chosen to satisfy certain "sufficient decrease" and "curvature" conditions, then this sequence of iterates is guaranteed to converge to a stationary point $\mathbf{x}_* \in \Omega$, provided the objective and constraints are smooth and bounded from below [37]. However, much work goes into finding a good α_k (involving several evaluations of the objective, constraints and their gradients) which also impacts their convergence rate.

Derivative-free methods also generate a sequence of iterates, except the iterates may depend on computing a search direction and step length (e.g., coordinate/pattern search [25]), or simplexes (e.g., Nelder-Mead [38]), or surrogate models (e.g., Bayesian optimization [10]), among others. Of course, these computations don't involve any higher-order information and, as a result, have to make more queries to the objective and constraints to compensate for it. Among the derivative-free methods, Bayesian optimization is particularly unique. It first involves the development of a probabilistic surrogate model of the objective (and constraints). Then, new iterates can be *optimally* chosen in the sense of maximizing the predicted utility of the new iterate. We provide a quick overview in the Appendix and the reader may refer to other sources for more details [47, 10, 51, 14].

2.1 Overview of the aerodynamic model

In this work, we leverage SU2 for high-fidelity aerodynamic calculations. SU2 is a finite-volume based open-source CFD and multi-physics simulation suite developed for solving

partial differential equations (PDEs) on unstructured meshes using numerical methods with adjoint capability [39]. We specifically leverage the inviscid (Euler) and Reynolds averaged Navier-Stokes (RANS) models within SU2. As all the test cases are in the transonic regime, the Jameson-Schmidt-Turkel (JST) scheme [20] is used for spatial discretization, which is a central scheme with 2nd order accuracy in time and space. Furthermore, an implicit Euler scheme is used for the time marching of the solution, as it is stable for any time-step size unlike the explicit scheme until a steady state is reached. For the RANS simulations, the popular one-equation Spalart-Allmaras (SA) turbulence model [53] is used as a closure for the system of equations. Slip wall boundary conditions and no-slip wall conditions are used to specify the aerodynamic surfaces in Euler simulations and RANS simulations respectively. In addition to that, a freestream boundary condition is applied to the farfield boundaries in each case and a symmetry boundary condition is used for the three-dimensional test cases to reduce the computational complexity. A constant CFL number of 50 is used in each case without any adaptation parameter. Further, W-cycle multigrid solver is used in the case of Euler simulations to accelerate convergence; however, this is not done for RANS simulations as it worsens the convergence of adjoint simulations, thereby negatively impacting the accurate computation of gradients of the objective function. Finally, we employ the minimum value of the $\log_{10}$ of the residual as the convergence criterion. This criterion is evaluated over the last 200 iterations of each simulation to ensure stability and consistency in the convergence assessment. Table 1 summarizes the three canonical geometries and their operating conditions considered in this study.

We use free form deformation (FFD) parametrization [50] in this work. The control point displacements on the FFD box are the design variables of the optimization problem; see Figure 1 for an illustration of the FFD parameterization and we provide a few more in the Appendix. The arrangement of control points is carefully designed to avoid influencing the deformation near critical regions such as the leading edge, trailing edge, wing root, and wing tip, thereby preserving the structural fidelity of the volume mesh in these sensitive areas. Additionally, as the control point displacements deform the geometry and the mesh, we apply necessary smoothing during deformation to ensure minimal mesh quality distortion; see the bottom of Figure 1.

The three test cases used in this work are summarized in Table 1. The NACA0012 mesh comprises 10216 unstructured triangular cells without any boundary layers. The RAE2822 mesh includes 22800 unstructured cells comprising of triangles and quadrilaterals. To capture the viscous phenomena, 26 additional layers of quad elements are added. The first layer of the boundary layer is placed approximately 1.008×10^{-5} m away from the wall such that the wall $y^+ \approx 1$. The 3D ONERA test case involves an unstructured mesh as well with 582752 elements.

Table 1: Summary of test cases.

Test Case	Mach	Reynolds ($\times 10^6$)	AOA (deg.)	Physics
NACA0012	0.85	∞	0.0	Euler
RAE2822	0.729	6.50	2.31	RANS
ONERAM6	0.8395	∞	3.06	Euler

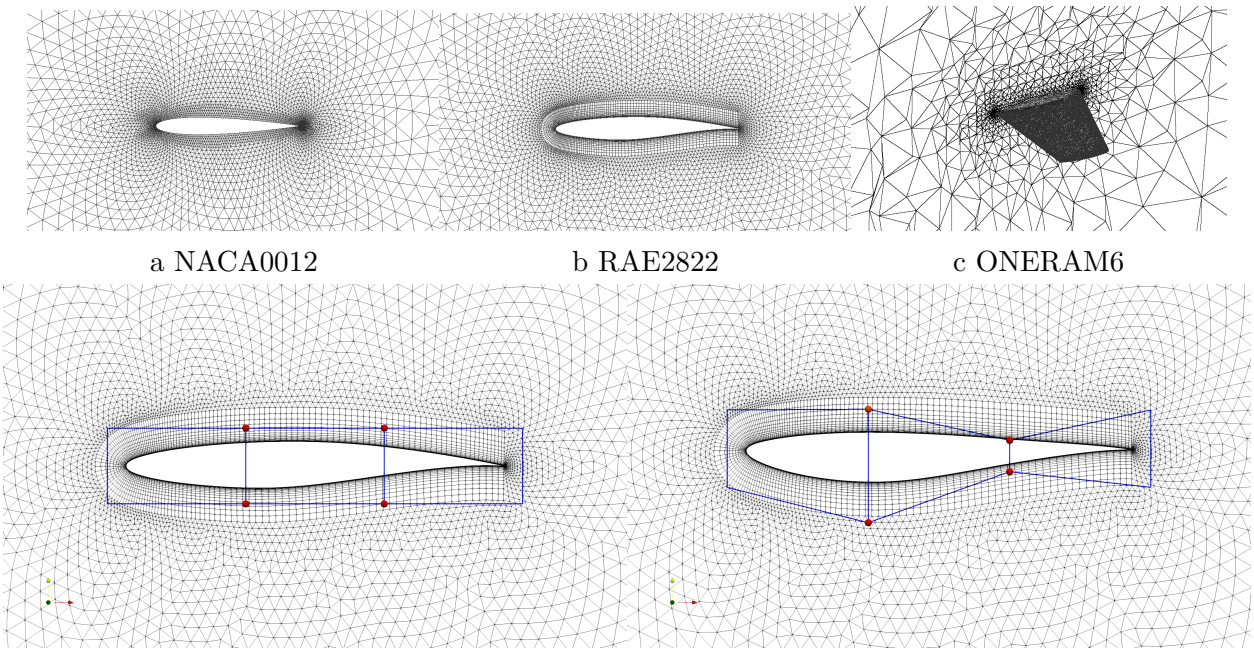

a NACA0012 b RAE2822 c ONERAM6

d Undeformed Mesh e Deformed Mesh

Figure 1: Computational mesh highlighting the near-field resolution.

2.2 Experiment design

To answer the central question of this work, we consider a combination of widely used derivative-based and derivative-free optimization algorithms. This includes the quasi-Newton method (`L-BFGS-B`) [58], first-order trust-region method (`Trust-constrained`) [6], truncated Newton conjugate gradient (`TNC`) [34], and sequential least squares quadratic programming (`SLSQP`) [12], for derivative-based methods. On the derivative-free side, we entertain Nelder-Mead (`NM`) [36], constrained optimization by linear approximation (`COBYLA`) [40], and Bayesian optimization (`BO`) with Gaussian process priors [44, 10, 11].

In all optimization runs, we use the following solver settings for each algorithm, that were held fixed across the experiments. For the `L-BFGS-B` and `Trust-constrained` methods, we set a gradient norm tolerance (gtol) of 10^{-4}, with `L-BFGS-B` also using a maximum number of iterations (maxiter) of 500. For the `NM` algorithm, we set the function absolute tolerance (fatol) to 10^{-4}. For the `SLSQP` method, we set ftol to 10^{-9}, to terminate the algorithm when the relative change in the objective function between successive iterations falls below this threshold. For the `TNC` method, we set the function tolerance (ftol) to 10^{-4} and gtol to 10^{-3}. For the `COBYLA` method, we set the convergence tolerance (tol) to 10^{-9} , terminating when both the maximum constraint violation and changes in the objective function become sufficiently small. Additionally, we normalize the design variables to be bounded by $[0, 1]$ to remove any undesirable influence of the scales of the design variables. We leverage the optimization routines within the open-source `SciPy` library.

Remark 4. Note that we don't restart the local optimization algorithms with a randomized choice of $\mathbf{x}_0$. Instead, $\mathbf{x}_0$ is chosen from the initial pool of seed points provided to `BO` that corresponds to the best feasible objective value.

For BO, we use the expected improvement (EI) acquisition function [23] for unconstrained problems and the scalable constrained Bayesian optimization (SCBO) [9] implementation for constrained problems, which combines Thompson sampling [54] with a trust-region method to select the iterates. All BO related code is implemented in the open-source library BoTorch [1]. All the code, including the SU2 mesh and configuration files, is available publicly [1] which will facilitate reproducing our results as well as further benchmarking.

For each unconstrained test case, the primary performance metrics include (i) the drag coefficient and (ii) the gradient infinity norm of the drag coefficient (for first-order optimality) versus optimization iteration and number of objective and gradient evaluations; we assume the cost of objective and gradient evaluations is roughly equal. For the constrained test cases, we additionally monitor the maximum constraint violation–this is the infinity norm of an aggregated vector of all constraint violations evaluated at an iterate. For Bayesian optimization, we compare the "best observed" (that is, the smallest feasible objective observed until the current iteration) drag coefficient at every iteration. Note that, unlike all other algorithms, BO requires an ensemble of "seed" points to start the algorithm; to account for this, BO convergence histories are offset to the right. We will provide further details in the following sections.

3 Results and discussion

3.1 Unconstrained NACA0012

We begin with the unconstrained optimization of NACA0012 under inviscid conditions. The control point displacements are contained to $[-0.1, 0.1]$; for example, with 4 control points, the domain $\mathcal{X} = [-0.1, 0.1]^4$. Figure 2 shows the drag coefficient (objective) history for 4, 8 and 16 control points; notice that derivative-based methods have highly varying performance—L-BFGS-B, SLSQP, and TNC rapidly converge to the minimum while Trust-constrained are relatively slow. This exemplifies the fact that derivative-based methods can vary drastically in performance depending on the search direction ($\mathbf{p}_k$) and step length (α_k) calculation. Derivative-free methods (NM and BO) take longer to converge, while still being quite comparable to TNC in the 4 control points case.

Note that, for BO , we show the max, min, and the average of 3 repetitions with randomized seed points. It is worth noting that BO costs one objective evaluation per iteration in contrast to other methods which can consume additional evaluations to compute the search step and gradient (when applicable). So, we compare convergence histories against the number of function (objective + gradient) evaluations in Figure 3. Now notice that BO performs comparably to derivative-based methods, while outperforming NM in the cases with 8 and 16 control points. It should be noted that we assign equal cost for objective function and adjoint evaluation costs; however, in practice, the adjoint solver in SU2 tends to take significantly longer times to converge, while occasionally failing to converge. Given these factors, we argue that BO is quite competitive for this 2D inviscid test case, despite not depending on gradient information.

[1] https://github.com/csdlpsu/aso

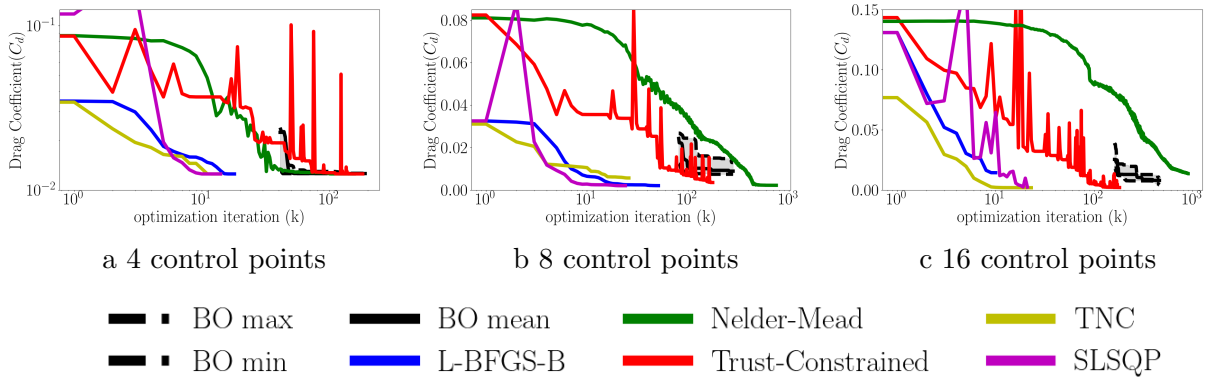

Figure 2: **Unconstrained NACA0012.** Convergence histories versus optimization iterations.

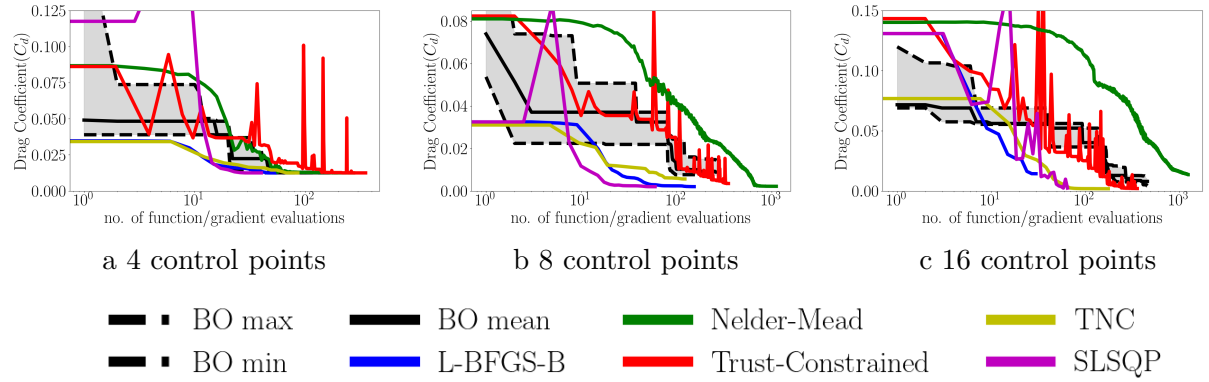

Figure 3: **Unconstrained NACA0012.** Convergence histories versus number of function/gradient evaluations.

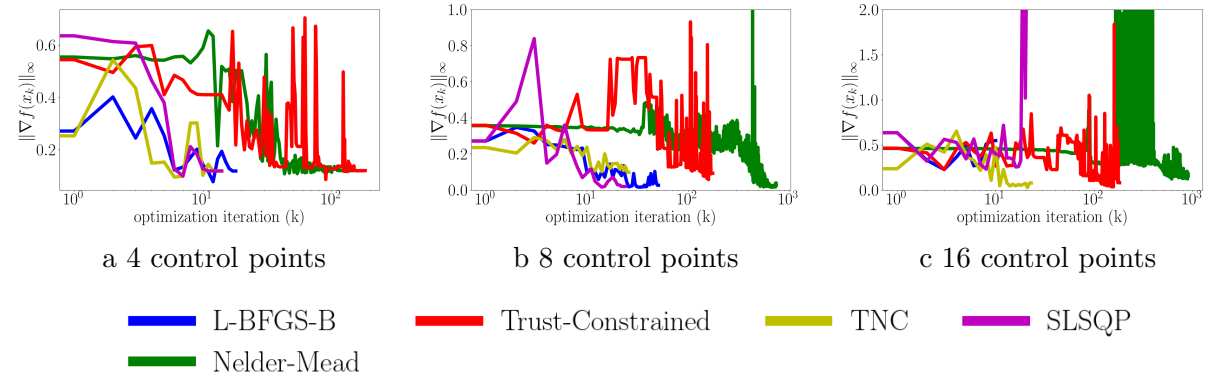

Figure 4: **Unconstrained NACA0012.** Gradient infinity norm history.

Finally, we also show the gradient infinity norm of the objective function in Figure 4. Notice that we don't achieve strict optimality ($\|\nabla f(\mathbf{x})\|_\infty = 0$) in any of the algorithms;

instead, the optimizer terminates after a few attempts to find a stationary point. Typically, the off-the-shelf optimizers are designed to terminate upon encountering diminishing returns in the objective function improvement. Furthermore, note that the gradient norm can drastically vary with iterations (particularly in `Trust-constrained`), which is likely exacerbated due to incomplete convergence of the adjoint solver. Therefore, we remark that in practice for aerodynamic design optimization problems, derivative-based optimizers don't always necessarily find a stationary point. Note that in Figure 4, we also include `NM`, where we manually compute the gradient (by calling the adjoint solver) at every step for comparison. This reveals that the variability in gradient norm, for derivative-based approaches, can be on par with that of derivative-free optimizers which do not seek a stationary point.

3.2 Unconstrained RAE2822

We now present the optimization results for RAE2822 under viscous conditions – this leads to more expensive forward and adjoint solver costs. The control point displacements are contained to $[-0.002, 0.002]$. Figure 5 shows the drag coefficient history for $4, 8, 16$, and 32 control points. Notice that derivative-free approaches (`NM` and `BO`) find the lowest objective value compared to all derivative-based approaches. `L-BFGS-B` and `TNC`, terminated early without achieving much reduction in the objective function. And, as in the NACA0012 experiment, the `Trust-constrained` objective history shows significantly more volatility than other methods. Further, we argue that the choice of initial point for derivative-based algorithms plays a major role in their convergence. On the other hand, despite the randomly chosen seed points for `BO`, their variability in performance (visualized as shaded gray in the figure) is quite acceptable for practical applications. Figure 6 shows the convergence history versus the number of function evaluations. Again, notice that the benefit of derivative-free methods is best demonstrated in this context. The derivative-based methods prematurely terminate with higher objective values despite utilizing expensive gradient and (quasi) $2nd$ order information. Finally, the gradient norm plots in Figure 7 show that strict optimality is not quite achieved in any of the algorithms, suggesting that the domain might not contain a stationary point or, potentially, the objective function is non-smooth. To verify this, we tested the same experiment with a different parametrization, namely the Hicks-Henne bump functions [17], shown in Figure 8. We observe that the gradient norm still plateaus at 10^{-1}, substantiating our claim.

3.3 Unconstrained ONERAM6

For the ONERAM6 test case, the approach is repeated, but considering the computational complexity and simulation time, we demonstrate the results for only one case considering 12 control points. The domain is set as $\mathcal{X} = [-0.00025, 0.00025]^{12}$. Figure 9 shows results for $M = 0.8395$ and $\alpha = 3.06$ degrees under inviscid conditions. The control points' placement and bounds are designed to ensure smooth wing deformation, avoiding any issues in the direct and adjoint simulations.

The convergence history of C_D with iteration is presented in Figure 9a. The trends observed for the derivative-based methods `L-BFGS-B` , `Trust-constrained` , and `TNC` , are consistent with the previous two test cases discussed in Section 3.1 and Section 3.2. However,

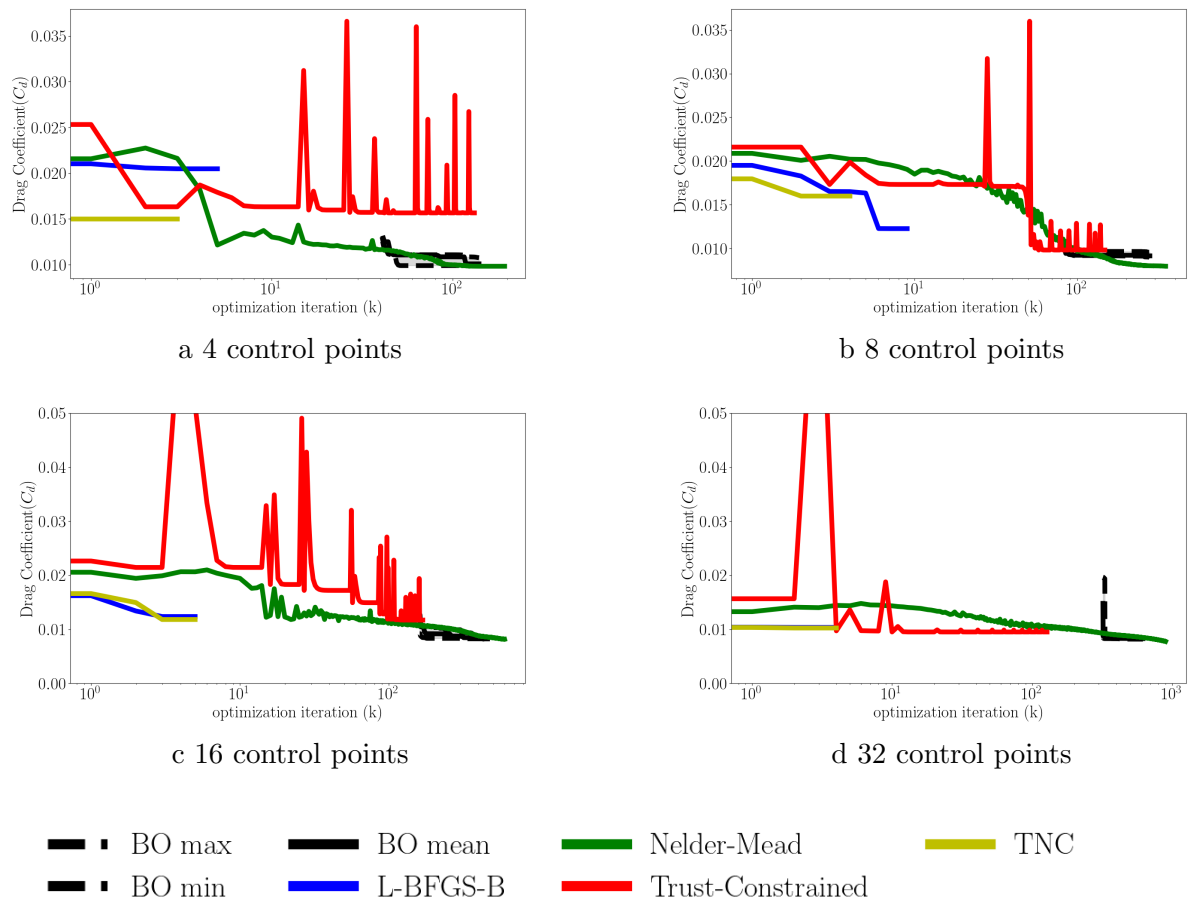

Figure 5: **Unconstrained RAE2822.** Convergence histories versus optimization iterations.

notice that BO finds the lowest objective value compared to all other methods. In terms of the number of function evaluations (right of Figure 9c), BO stands out by demonstrating the fastest convergence.

3.4 Constrained RAE2822

The optimization problem we considered for this experiment can be formulated as described in Equation 3.

$$\begin{aligned} \min_{\mathbf{x}\in\mathcal{X}} \quad & C_d \\ \text{s.t.} \quad & C_{mz} \leq 0.092, \\ & C_l = 0.75, \\ & t_{\max} \geq 0.12, \end{aligned} \tag{3}$$

where C_{mz} denotes the pitching moment coefficient of the airfoil about the quarter-chord, C_l denotes the lift coefficient, and $t_{\max}$ denotes the maximum airfoil thickness-to-chord ratio.

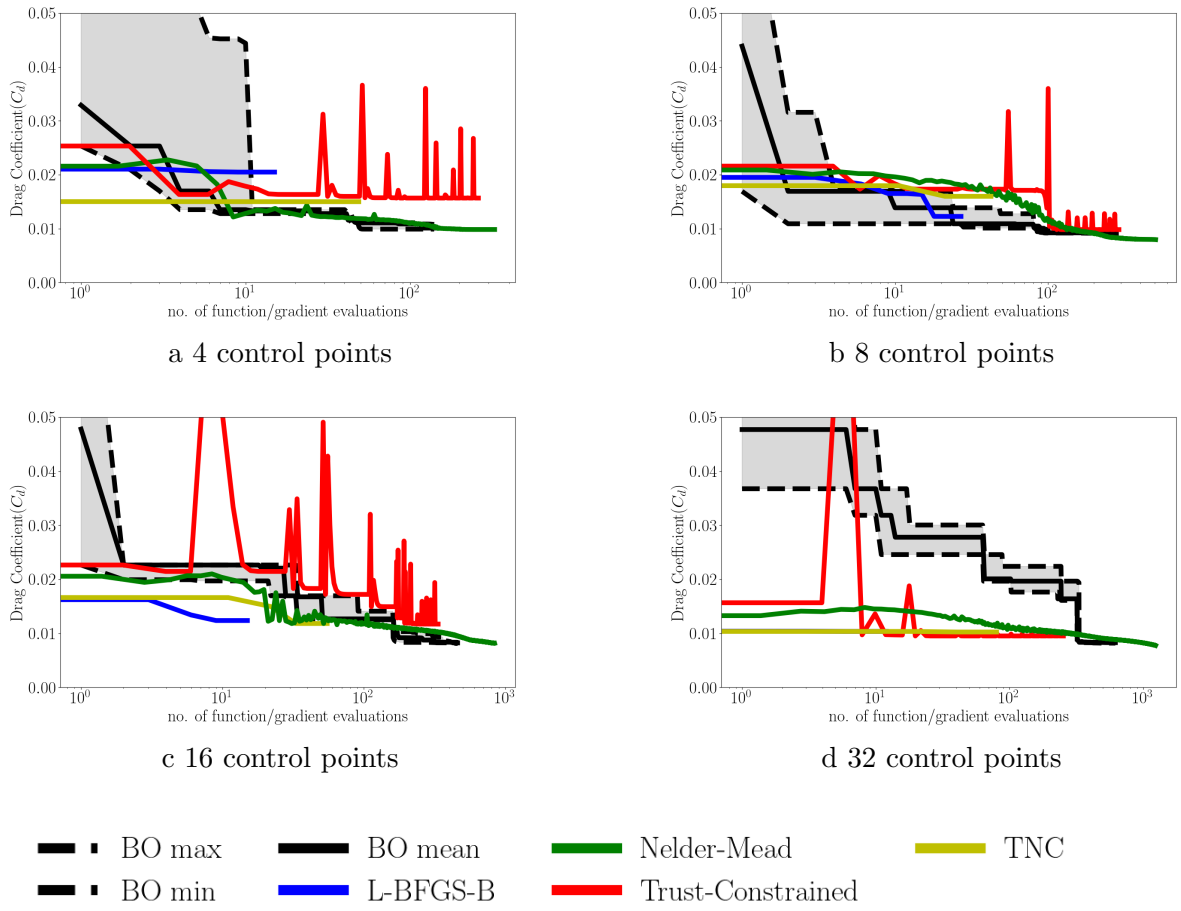

Figure 6: **Unconstrained RAE2822.** Convergence histories versus number of function/gradient evaluations.

The optimization results are shown in figures 10, 11, and 12. In terms of the objective function, notice that derivative-free methods, `COBYLA` and `BO`, give the lowest objective values among all the methods compared; particularly, `COBYLA` and `BO` are quite similar in performance. The maximum constraint violation (MCV) is shown in Figure 12. Notice that `Trust-constrained` can sometimes (4 control points) fail to find a feasible solution in the constrained setting. In contrast, `BO` constantly attempts to balance exploration and exploitation–as a result, infeasible iterates are still acceptable as they help improve the GP surrogate models. However, for the objective function plots (Figure 10a, 10b and 10c), we only show the best feasible objective value.

Notice that the history of MCV directly correlates with the convergence behavior of the objective derivative-based algorithms. `SLSQP` experiences extreme constraint violations in early iterations, particularly for high-dimensional cases where MCV spikes coincide with C_d oscillations, highlighting its struggle to maintain feasibility while reducing drag. However, it rapidly improves feasibility, requiring fewer iterations to converge. `Trust-constrained` maintains the lowest MCV across all cases, demonstrating better constraint handling, but its

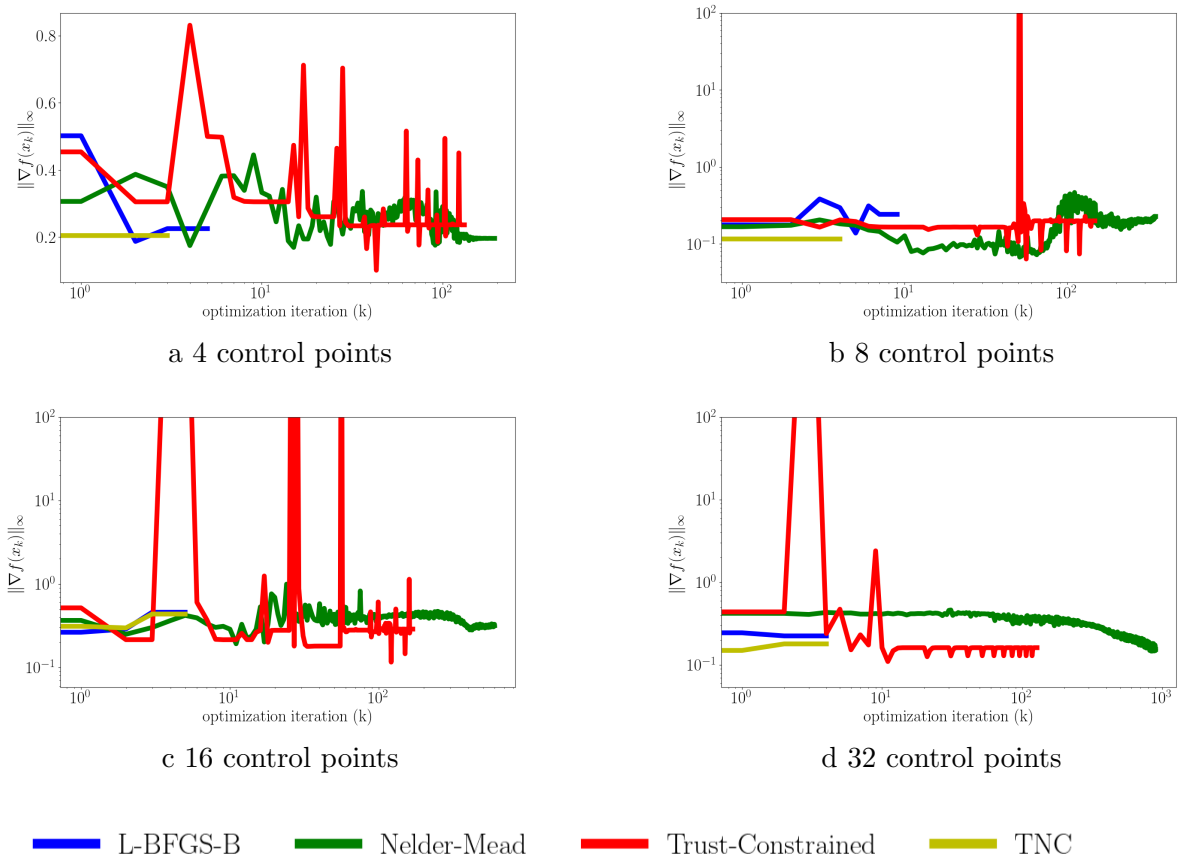

Figure 7: **Unconstrained RAE2822.** Gradient infinity norm history.

conservative approach limits C_d reduction. `COBYLA` shows a moderate decline in constraint violations, resulting in slower convergence. `BO` , on the other hand, achieves the best balance between constraint satisfaction and objective function improvement, avoiding extreme MCV spikes seen in other methods, especially in high-dimensional cases, though occasional constraint violations slow its overall convergence.

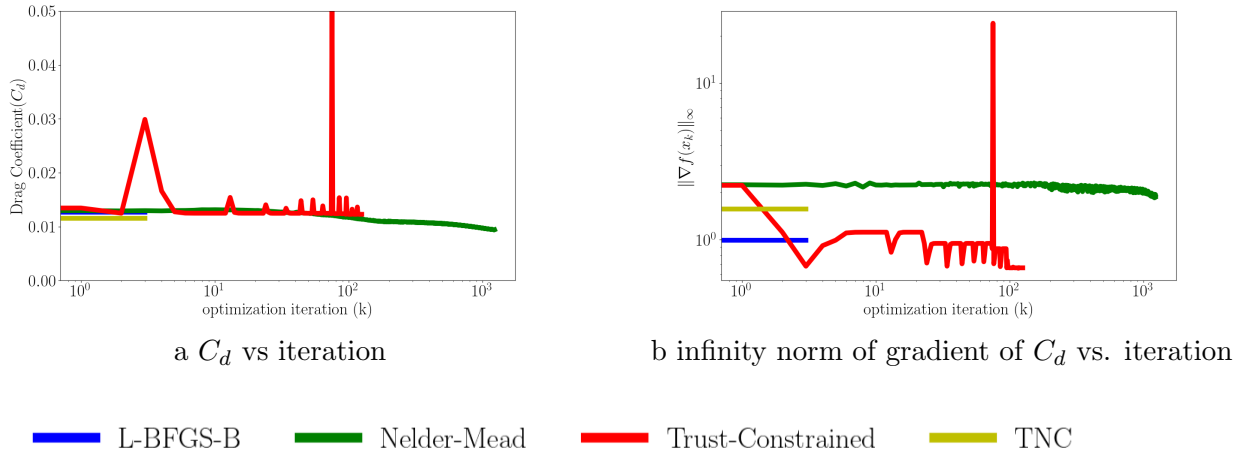

a C_d vs iteration

b infinity norm of gradient of C_d vs. iteration

Figure 8: **Unconstrained RAE2822.** Convergence histories Hicks and Henne parametrization.

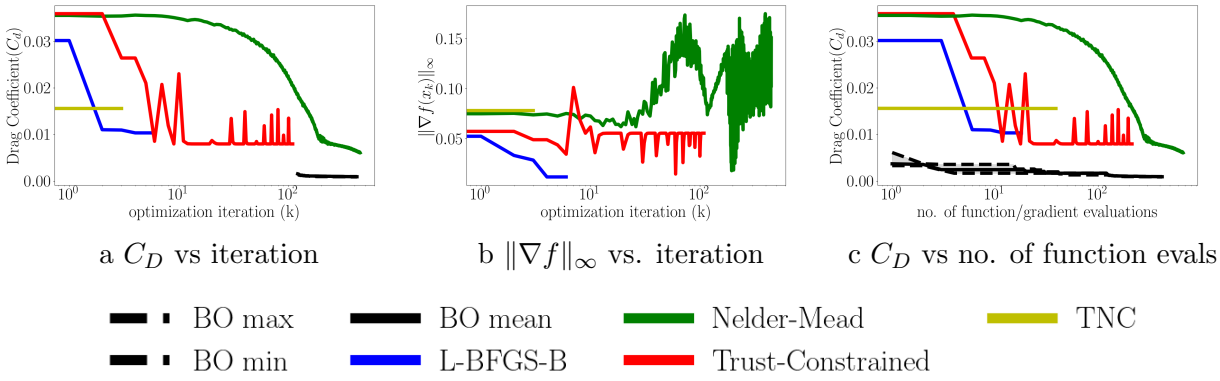

a C_D vs iteration

b $\|\nabla f\|_\infty$ vs. iteration

c C_D vs no. of function evals

Figure 9: **Unconstrained ONERAM6.** Convergence histories versus number of function/gradient evaluations.

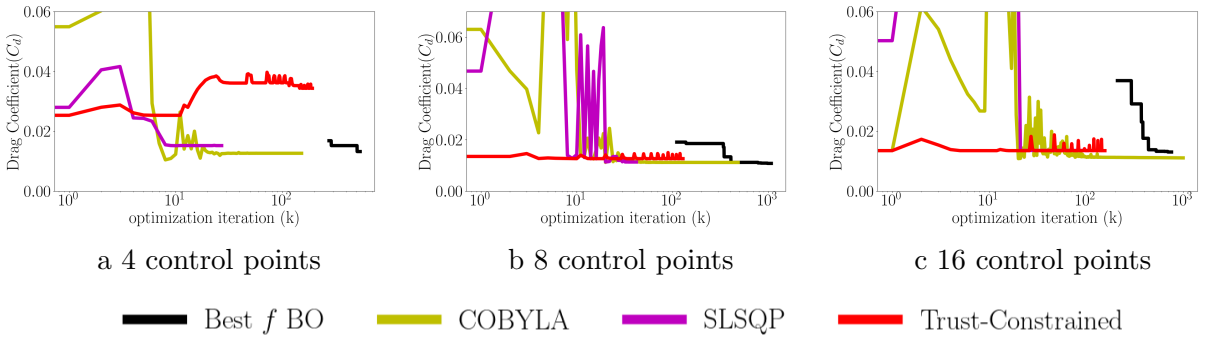

a 4 control points

b 8 control points

c 16 control points

Figure 10: **Constrained RAE2822.** Convergence histories versus optimization iterations.

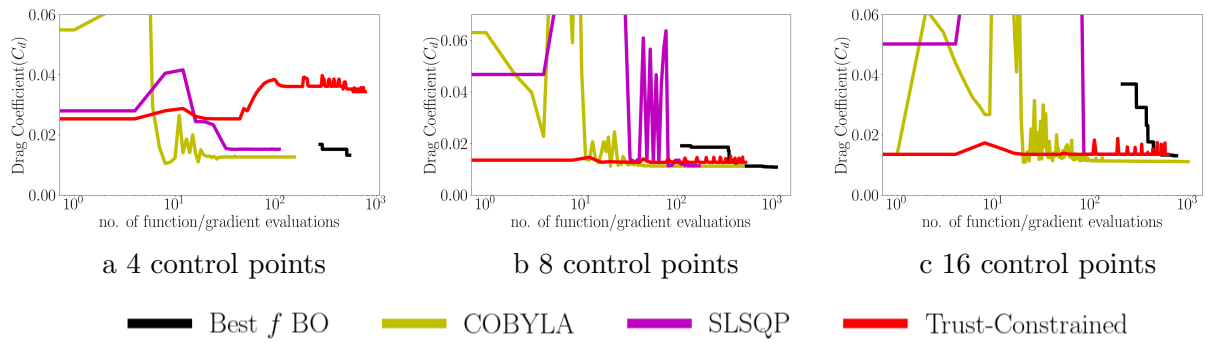

Figure 11: **Constrained RAE2822.** Convergence histories versus number of function/gradient evaluations.

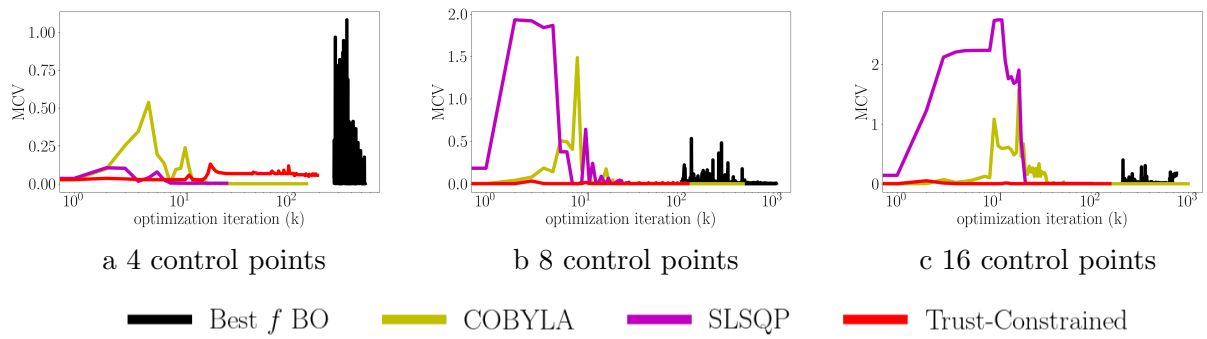

Figure 12: **Constrained RAE2822.** Convergence histories of MCV.

3.5 Constrained ONERA M6

Finally, we present results on the constrained optimization of ONERAM6 under inviscid conditions. The optimization problem is described in Equation 4.

$$\begin{aligned} \min_{\mathbf{x}\in\mathcal{X}} \quad & C_D \\ \text{s.t.} \quad & t_1 \geq 0.078, \\ & t_2 \geq 0.072, \\ & t_3 \geq 0.066, \\ & t_4 \geq 0.061, \\ & t_5 \geq 0.055, \\ & C_L = 0.292, \end{aligned} \tag{4}$$

where t_i represents the thickness-to-chord ratio at the ith spanwise location and C_L represents the lift coefficient.

Figure 13a illustrates the convergence history of the objective (C_D). Again, notice that derivative-free methods outperform derivative-based methods, with `BO` outperforming `COBYLA` by demonstrating faster convergence. The MCV plot shows that all methods find a

feasible solution relatively quickly (within ~ 20 iterations), including `COBYLA`. This experiment further demonstrates that derivative-free methods can outperform derivative-based methods for three-dimensional problems with higher dimensional parametrization.

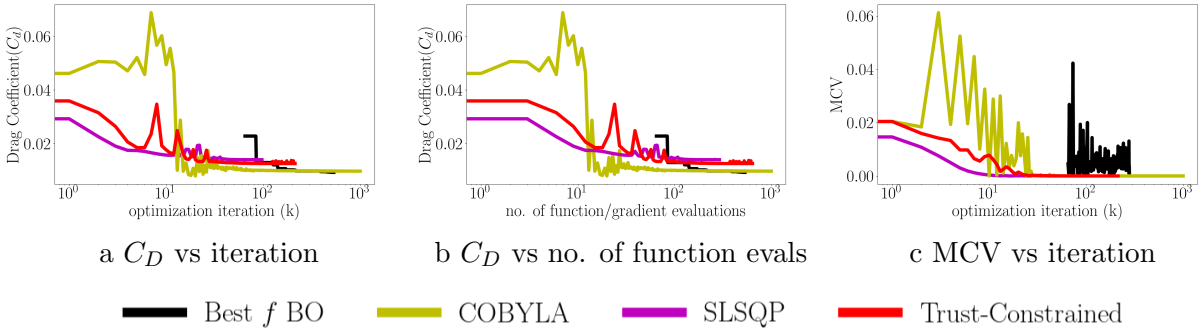

Figure 13: **Constrained ONERAM6.** Convergence histories.

4 Conclusions and future work

We present the first of a sequence of studies aimed at evaluating the feasibility of derivative-free optimization methods for practical aerodynamic design optimization problems. To our knowledge, a systematic benchmarking of derivative-free approaches against derivative-based methods doesn't exist – this work fills that gap. Based on two airfoil and one wing test case, up to 32 dimensions, we benchmark three derivative-free algorithms (`NM`, `COBYLA`, and `BO`) against four derivative-based approaches (`L-BFGS-B`, `SLSQP`, `Trust-constrained`, `TNC`), with and without constraints. Our experiments reveal that the additional cost invested in computing gradients does not necessarily translate into efficient convergence to a stationary point; indeed, in a majority of our experiments, we observe derivative-based methods fail to achieve first-order optimality. Furthermore, in the constrained setting, derivative-based methods also don't always find feasible designs. Overall, from an objective minimization and reducing the budget of queries to an expensive aerodynamic model perspective, derivative-free methods perform quite competitively while frequently outperforming derivative-based methods. We note that for some of the derivative-based algorithms, we are conservative in estimating the number of function and gradient evaluations to be two per iteration—in practice, computing line search step lengths can cost much more than that [37]. Despite this, a competitive performance demonstrated by derivative-free methods provides substantial evidence, at least in moderate dimensions, that they are a realistic option for practical aerodynamic design optimization. Crucially, surrogate-based methods such as `BO` are particularly attractive due to their automatic ability to balance exploration and exploitation, despite only depending on zeroth-order information. It is worth noting that `BO` offers further flexibility, in terms of the surrogate model and acquisition policy choices, that provides scope for further improvement in performance.

Naturally, one of the primary directions of future work is to perform the same study in higher dimensions to observe if the conclusions still hold. While it is known that global

surrogate models, such as GPs, scale poorly with dimensions, several measures already exist to scale them to high dimensions [8, 9, 26, 56, 35, 30, 47]. We plan on leveraging existing methods to benchmark `BO` on high-dimensional aerodynamic design optimization problems. Another direction of future work is to evaluate the use of non-stationary surrogates (e.g., deep Gaussian processes [2, 3, 42, 43]) for their potential to improve `BO` performance.

5 Statements and declarations

- **Funding.** N/A
- **Conflict of Interest.** The authors have no conflicts of interest to disclose.
- **Author contributions.** P. Plaban – CFD preparation and analysis, derivative-based algorithms, manuscript drafting. P. Bachman – CFD analysis and derivative-free algorithms. A. Renganathan – design of experiments, manuscript drafting, and research supervision.
- **Data Availability.** N/A
- **Ethics approval and Consent to participate.** Yes
- **Replication of Results.** Code publicly available at `https://github.com/csdlpsu/aso`.

Appendix

5.1 Bayesian optimization with Gaussian process priors

We place a GP prior on the oracle $f(\mathbf{x}) \sim \mathcal{GP}(0, k(\mathbf{x}, \cdot))$, where $k(\cdot,\cdot) : \boldsymbol{\mathcal{X}} \times \boldsymbol{\mathcal{X}} \to \mathbb{R}_+$ is a covariance function (a.k.a., *kernel*). We denote the observations from the oracle as $y_i = f(\mathbf{x}_i) + \epsilon_i,\ i = 1, \ldots, n$, where we assume that ϵ_i is a zero-mean Gaussian with unknown variance τ^2. We begin by fitting a posterior GP (parametrized by hyperparameters $\boldsymbol{\Omega}$) for the observations $\boldsymbol{\mathcal{D}}_n = \{\mathbf{x}_i, y_i, \tau^2\},\ i = 1, \ldots, n$, which gives the conditional aposteriori distribution [44]:

$$
\begin{aligned}
Y(\mathbf{x})|\boldsymbol{\mathcal{D}}_n, \boldsymbol{\Omega} &\sim \mathcal{GP}(\mu_n(\mathbf{x}), \sigma_n^2(\mathbf{x})), \\
\mu_n(\mathbf{x}) &= \mathbf{k}_n^\top [\mathbf{K}_n + \tau^2 \mathbf{I}]^{-1} \mathbf{y}_n \\
\sigma_n^2(\mathbf{x}) &= k(\mathbf{x}, \mathbf{x}) - \mathbf{k}_n^\top [\mathbf{K}_n + \tau^2 \mathbf{I}]^{-1} \mathbf{k}_n,
\end{aligned} \tag{5}
$$

where $\mathbf{k}_n \equiv k(\mathbf{x}, X_n)$ is a vector of covariances between $\mathbf{x}$ and all observed points in $\boldsymbol{\mathcal{D}}_n$, $\mathbf{K}_n \equiv k(X_n, X_n)$ is a sample covariance matrix of observed points in $\boldsymbol{\mathcal{D}}_n$, $\mathbf{I}$ is the identity matrix, and $\mathbf{y}_n$ is the vector of all observations in $\boldsymbol{\mathcal{D}}_n$. We also denote by $X_n = [\mathbf{x}_1, \ldots, \mathbf{x}_n]^\top \in \mathbb{R}^{n \times d}$ the observation sites. BO seeks to make sequential decisions based on a probabilistic utility function constructed out of the posterior GP $u(\mathbf{x}) = u(Y(\mathbf{x})|\boldsymbol{\mathcal{D}}_n)$. Sequential decisions are the result of an "inner" optimization subproblem that optimizes an acquisition function, typically,

Algorithm 1 Generic Bayesian optimization

Given: $\boldsymbol{\mathcal{D}}_n = \{\mathbf{x}_i, y_i\}_{i=1}^n$, total budget B, and GP hyperparameters $\boldsymbol{\Omega}$

Result: $\{\max_{i=1,\ldots,B} y_i, \ \arg\max_{i=1,\ldots,B} f(\mathbf{x}_i), \}$

for $i = n+1, \ldots, B,$ **do**

  Find $\mathbf{x}_i \in \arg\max_{\mathbf{x}\in\boldsymbol{\mathcal{X}}} \alpha(\mathbf{x})$ (acquisition function maximization)

  Observe $y_i = f(\mathbf{x}_i) + \epsilon_i$

  Append $\boldsymbol{\mathcal{D}}_i = \boldsymbol{\mathcal{D}}_{i-1} \cup \{\mathbf{x}_i, y_i\}$

  Update GP hyperparameters $\boldsymbol{\Omega}$

of the form $\alpha(\mathbf{x}) = \mathbb{E}_{Y|\boldsymbol{\mathcal{D}}_n}[u(Y(\mathbf{x}))]$. For example, the EI [23] and PI [33] can be expressed as $\alpha_{\text{PI}}(\mathbf{x}) = \mathbb{E}_{Y|\boldsymbol{\mathcal{D}}_n}[(Y(\mathbf{x}) - \xi)]$ and $\alpha_{\text{EI}}(\mathbf{x}) = \mathbb{E}_{Y|\boldsymbol{\mathcal{D}}_n}[\max(0, (Y(\mathbf{x}) - \xi))]$, respectively,

$$\begin{aligned}\alpha_{\text{PI}}(\mathbf{x}) =& \mathbb{E}_{Y|\boldsymbol{\mathcal{D}}_n}[(Y(\mathbf{x}) - \xi)]\\ \alpha_{\text{EI}}(\mathbf{x}) =& \mathbb{E}_{Y|\boldsymbol{\mathcal{D}}_n}[\max(0, (Y(\mathbf{x}) - \xi))],\end{aligned}$$

where ξ is a target value. Although α_{EI} and α_{PI} have analytically closed and continuously differentiable forms, their batch-acquisition variants are not necessarily [13]. Further, the information-theoretic approaches [15, 16, 55] also typically require approximations and/or Monte Carlo sampling, making them computationally expensive and hard to optimize. We provide a generic `BO` algorithm in Algorithm 1.

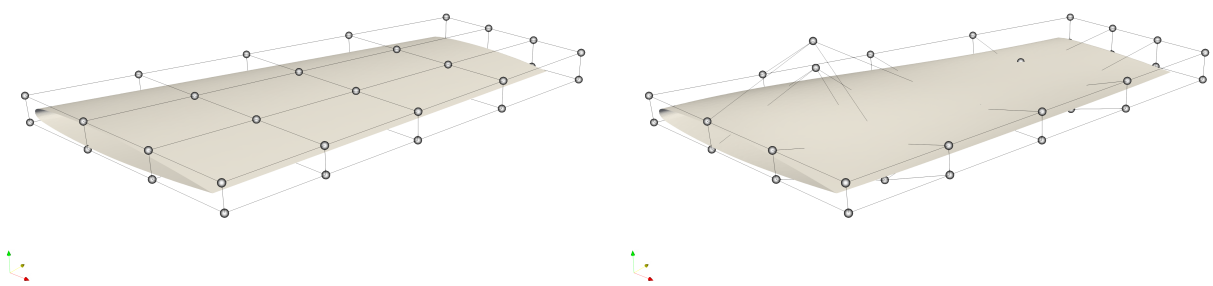

Figure 14: Illustration of the FFD parametrization on the ONERAM6 wing. Left and right show an undeformed and deformed wing, respectively. Note that only a subset of the control points are treated as design variables – the rest are held fixed. Notice that drastic displacement in the control point don't necessarily result in drastic shape deformations, due to the smoothing applied to the shapes.

References

[1] Maximilian Balandat, Brian Karrer, Daniel R Jiang, Samuel Daulton, Benjamin Letham, Andrew Gordon Wilson, and Eytan Bakshy. BoTorch: Programmable Bayesian optimization in PyTorch. *arXiv:1910.06403*, 2019.

[2] Annie S Booth, Robert Gramacy, and Ashwin Renganathan. Actively learning deep gaussian process models for failure contour and probability estimation. In *AIAA SCITECH 2024 Forum*, page 0577, 2024.

[3] Annie S Booth, S Ashwin Renganathan, and Robert B Gramacy. Contour location for reliability in airfoil simulation experiments using deep gaussian processes. *The Annals of Applied Statistics*, 19(1):191–211, 2025.

[4] Maziar A. Bouhlel, Nicolas Bartoli, John T. Hwang, Renaud Lafage, Joseph Morlier, and Joaquim R. R. A. Martins. A scalable approach for high-dimensional surrogate modeling with applications to aerodynamic shape optimization. *AIAA Journal*, 58(9): 3888–3902, 2020. doi: 10.2514/1.J058853.

[5] Wei Chen, Kevin Chiu, and Mark Fuge. Aerodynamic design optimization and shape exploration using generative adversarial networks. In *AIAA SciTech Forum*, 2019. doi: 10.2514/6.2019-2351.

[6] Andrew R. Conn, Nicholas I. M. Gould, and Philippe L. Toint. *Trust Region Methods*. Society for Industrial and Applied Mathematics (SIAM), Philadelphia, PA, 2000. ISBN 978-0-89871-460-9. doi: 10.1137/1.9780898719857.

[7] Racheal M. Erhard and Juan J. Alonso. Multi-fidelity bayesian optimization of a coaxial rotor for evtol aircraft. In *AIAA SciTech Forum*, 2024. doi: 10.2514/6.2024-2506.

[8] David Eriksson and Martin Jankowiak. High-dimensional bayesian optimization with sparse axis-aligned subspaces. In *Uncertainty in Artificial Intelligence*, pages 493–503. PMLR, 2021.

[9] David Eriksson, Michael Pearce, Jacob Gardner, Ryan D Turner, and Matthias Poloczek. Scalable global optimization via local bayesian optimization. *Advances in neural information processing systems*, 32, 2019.

[10] Peter I. Frazier. A tutorial on bayesian optimization. *arXiv preprint arXiv:1807.02811*, 2018. doi: 10.48550/arXiv.1807.02811.

[11] Roman Garnett. *Bayesian Optimization*. Cambridge University Press, 2023. ISBN 9781108425780. doi: 10.1017/9781108348973.

[12] Philip E. Gill, Walter Murray, and Margaret H. Wright. *Practical Optimization*. SIAM, 2019. doi: 10.1137/1.9781611975604.

[13] David Ginsbourger and Rodolphe Le Riche. Towards Gaussian process-based optimization with finite time horizon. In *Contributions to Statistics*, pages 89–96. Springer, 2010. doi: 10.1007/978-3-7908-2410-0_12.

[14] Stewart Greenhill, Santu Rana, Sunil Gupta, Pratibha Vellanki, and Svetha Venkatesh. Bayesian optimization for adaptive experimental design: A review. *IEEE access*, 8: 13937–13948, 2020.

[15] Daniel Hernández-Lobato, José Miguel Hernández-Lobato, Amar Shah, and Ryan P Adams. Predictive Entropy Search for Multi-objective Bayesian Optimization.

[16] José Miguel Hernández-Lobato, Matthew W. Hoffman, and Zoubin Ghahramani. Predictive entropy search for efficient global optimization of black-box functions. In *Advances in Neural Information Processing Systems*, pages 918–926, 2014.

[17] Raymond M. Hicks and Peter A. Henne. Wing design by numerical optimization. *Journal of Aircraft*, 15(7):407–412, 1978. doi: 10.2514/3.58379.

[18] W. M. Hsu, J. F. Hughes, and H. Kaufman. Direct manipulation of free-form deformations. *ACM SIGGRAPH Computer Graphics*, 26(2):177–184, 1992. doi: 10.1145/142920.134036.

[19] A. Jameson. Aerodynamic design via control theory. *Journal of Scientific Computing*, 3 (3):233–260, 1988. doi: 10.1007/BF01061285.

[20] Antony Jameson. The origins and further development of the jameson-schmidt-turkel (jst) scheme. In *AIAA Aviation 2015*, Dallas, Texas, 2015. American Institute of Aeronautics and Astronautics. doi: 10.2514/6.2015-2457. AIAA Paper 2015-2457.

[21] Timothy M. S. Jim, Ghifari A. Faza, Pramudita S. Palar, and Koji Shimoyama. Bayesian optimization of a low-boom supersonic wing planform. *AIAA Journal*, 59(11):4514–4529, 2021. doi: 10.2514/1.J060225.

[22] D. R. Jones, C. D. Perttunen, and B. E. Stuckman. Lipschitzian optimization without the lipschitz constant. *Journal of Optimization Theory and Applications*, 79(1):157–181, 1993. doi: 10.1007/BF00941892.

[23] Donald R. Jones, Matthias Schonlau, and William J. Welch. Efficient global optimization of expensive black-box functions. *Journal of Global Optimization*, 13(4):455–492, 1998. doi: 10.1023/A:1008306431147.

[24] Abhishek Kundu, H. G. Matthies, and M. I. Friswell. Probabilistic optimization of engineering systems with prescribed target design in a reduced parameter space. *Computational Methods in Applied Mechanics and Engineering*, 339:640–660, 2018. doi: 10.1016/j.cma.2018.03.041.

[25] Robert Michael Lewis and Virginia Torczon. Pattern search algorithms for bound constrained minimization. *SIAM Journal on optimization*, 9(4):1082–1099, 1999.

[26] Chun-Liang Li, Kirthevasan Kandasamy, Barnabás Póczos, and Jeff Schneider. High dimensional bayesian optimization via restricted projection pursuit models. In *Artificial Intelligence and Statistics*, pages 884–892. PMLR, 2016.

[27] Jichao Li, Mengqi Zhang, Joaquim R. R. A. Martins, and Chang Shu. Efficient aerodynamic shape optimization with deep-learning-based geometric filtering. *AIAA Journal*, 58(10):4243–4259, 2020. doi: 10.2514/1.J059254.

[28] Jichao Li, Xiaosong Du, and Joaquim R. R. A. Martins. Machine learning in aerodynamic shape optimization. *Progress in Aerospace Sciences*, 134:100849, 2022. doi: 10.1016/j.paerosci.2022.100849.

[29] Ruo-Lin Liu, Qiang Zhao, Xian-Jun He, Xin-Yi Yuan, Wei-Tao Wu, and Ming-Yu Wu. Airfoil optimization based on multi-objective bayesian optimization. *Journal of Mechanical Science and Technology*, 36(11):5561–5573, 2022. doi: 10.1007/s12206-022-1020-y.

[30] Daniel James Lizotte. Practical bayesian optimization. 2008.

[31] André L. Marchildon and David W. Zingg. Gradient-enhanced bayesian optimization with application to aerodynamic shape optimization. In *AIAA Aviation Forum and ASCEND 2024*, 2024. doi: 10.2514/6.2024-4405.

[32] Azzurra Meo, Alessandro Aponte, Alessandro Munafò, Giulio Gori, and Marco Panesi. A bayesian framework for the shape optimization of atmospheric reentry vehicles. In *AIAA Aviation Forum and ASCEND, 2024*. American Institute of Aeronautics and Astronautics Inc, AIAA, 2024. doi: 10.2514/6.2024-3563.

[33] Jonas Mockus, Vytautas Tiešis, and Antanas Žilinskas. The application of Bayesian methods for seeking the extremum. *Towards Global Optimization*, 2:117–129, 1978.

[34] Stephen G. Nash. Newton-type minimization via the lanczos method. *SIAM Journal on Numerical Analysis*, 21(4):770–788, 1984. doi: 10.1137/0721050.

[35] Amin Nayebi, Alexander Munteanu, and Matthias Poloczek. A framework for bayesian optimization in embedded subspaces. In *International Conference on Machine Learning*, pages 4752–4761. PMLR, 2019.

[36] J. A. Nelder and R. Mead. A simplex method for function minimization. *The Computer Journal*, 7(4):308–313, 1965. doi: 10.1093/comjnl/7.4.308.

[37] Jorge Nocedal and Stephen J Wright. *Numerical optimization*. Springer, 1999.

[38] Donald M Olsson and Lloyd S Nelson. The nelder-mead simplex procedure for function minimization. *Technometrics*, 17(1):45–51, 1975.

[39] Francisco Palacios, Juan Alonso, Karthikeyan Duraisamy, Michael Colonno, Jason Hicken, Aniket Aranake, Alejandro Campos, Sean Copeland, Thomas Economon, Amrita Lonkar, Trent Lukaczyk, and Thomas Taylor. Stanford University Unstructured (SUˆ2): An open-source integrated computational environment for multi-physics simulation and design. In *51st AIAA Aerospace Sciences Meeting including the New Horizons Forum and Aerospace Exposition*. American Institute of Aeronautics and Astronautics, 2013. doi: 10.2514/6.2013-287.

[40] M. J. D. Powell. A direct search optimization method that models the objective and constraint functions by linear interpolation. In S. Gomez and J.-P. Hennart, editors, *Advances in Optimization and Numerical Analysis*, volume 275 of *Mathematics and Its Applications*, pages 51–67. Springer, 1994. doi: 10.1007/978-94-015-8330-5_4.

[41] Nestor V. Queipo, Raphael T. Haftka, Wei Shyy, Tapabrata Goel, Rajiv Vaidyanathan, and Paul K. Tucker. Surrogate-based analysis and optimization. *Progress in Aerospace Sciences*, 41(1):1–28, 2005. doi: 10.1016/j.paerosci.2005.02.001.

[42] Dushhyanth Rajaram, Tejas G Puranik, Ashwin Renganathan, Woong Je Sung, Olivia J Pinon-Fischer, Dimitri N Mavris, and Arun Ramamurthy. Deep gaussian process enabled surrogate models for aerodynamic flows. In *AIAA scitech 2020 forum*, page 1640, 2020.

[43] Dushhyanth Rajaram, Tejas G Puranik, S Ashwin Renganathan, WoongJe Sung, Olivia Pinon Fischer, Dimitri N Mavris, and Arun Ramamurthy. Empirical assessment of deep gaussian process surrogate models for engineering problems. *Journal of Aircraft*, 58(1):182–196, 2021.

[44] Carl Edward Rasmussen and Christopher K. I. Williams. *Gaussian Processes for Machine Learning*. The MIT Press, 2006. ISBN 9780262182539. doi: https://doi.org/10.7551/mitpress/3206.001.0001.

[45] Thomas A. Reist, David Koo, David W. Zingg, Pascal Bochud, Philippe Castonguay, and David Leblond. Cross-validation of high-fidelity aerodynamic shape optimization methodologies for aircraft wing-body optimization. *AIAA Journal*, 58(6):2581–2595, 2020. doi: 10.2514/1.J059091.

[46] Ashwin Renganathan. Efficient reliability analysis with multifidelity gaussian processes and normalizing flows. In *AIAA SCITECH 2024 Forum*, page 0576, 2024.

[47] Ashwin Renganathan and Kade Carlson. qpots: Efficient batch multiobjective bayesian optimization via pareto optimal thompson sampling. In *International Conference on Artificial Intelligence and Statistics*, pages 4051–4059. PMLR, 2025.

[48] S Ashwin Renganathan, Romit Maulik, and Jai Ahuja. Enhanced data efficiency using deep neural networks and gaussian processes for aerodynamic design optimization. *Aerospace Science and Technology*, 111:106522, 2021. doi: 10.1016/j.ast.2021.106522.

[49] S Ashwin Renganathan, Vishwas Rao, and Ionel M Navon. Camera: A method for cost-aware, adaptive, multifidelity, efficient reliability analysis. *Journal of Computational Physics*, 472:111698, 2023.

[50] Thomas W. Sederberg and Scott R. Parry. Free-form deformation of solid geometric models. *SIGGRAPH Computer Graphics*, 20(4):151–160, 1986. doi: 10.1145/15886.15903.

[51] Bobak Shahriari, Kevin Swersky, Ziyu Wang, Ryan P Adams, and Nando De Freitas. Taking the human out of the loop: A review of bayesian optimization. *Proceedings of the IEEE*, 104(1):148–175, 2015.

[52] Haris Moazam Sheikh, Tess A. Callan, Kealan J. Hennessy, and Philip S. Marcus. Optimization of the shape of a hydrokinetic turbine's draft tube and hub assembly using design-by-morphing with bayesian optimization. *Computer Methods in Applied Mechanics and Engineering*, 401:115654, 2022. doi: 10.1016/j.cma.2022.115654.

[53] Philippe R. Spalart and Steven R. Allmaras. A one-equation turbulence model for aerodynamic flows. *AIAA Journal*, 30(4):439–446, 1992. doi: 10.2514/3.10416.

[54] William R Thompson. On the likelihood that one unknown probability exceeds another in view of the evidence of two samples. *Biometrika*, 25(3-4):285–294, 1933.

[55] Zi Wang and Stefanie Jegelka. Max-value entropy search for efficient Bayesian optimization. In *Proceedings of the 34th International Conference on Machine Learning*, volume 70, pages 3627–3635, 2017.

[56] Ziyu Wang, Frank Hutter, Masrour Zoghi, David Matheson, and Nando De Feitas. Bayesian optimization in a billion dimensions via random embeddings. *Journal of Artificial Intelligence Research*, 55:361–387, 2016.

[57] D. Y. Xu, Y. Shen, W. Huang, Z. Y. Guo, H. Zhang, and D. F. Xu. Parametric modelling and variable-fidelity bayesian optimization of aerodynamics for a reusable flight vehicle. *Fluid Dynamics*, 59(6):123–135, 2024. doi: 10.1134/S0015462824603814.

[58] Ciyou Zhu, Richard H. Byrd, Peihuang Lu, and Jorge Nocedal. Algorithm 778: L-bfgs-b: Fortran subroutines for large-scale bound-constrained optimization. *ACM Transactions on Mathematical Software*, 23(4):550–560, 1997. doi: 10.1145/279232.279236.